A MULTI-WAVELENGTH STUDY

OF THE HOT COMPONENT OF THE INTERSTELLAR MEDIUM

NASA Grant NAG5-8483

Annual Report

For the Period 1 April 2001 through 31 March 2002

Principal Investigator
Dr. Joy Nichols

March 2002

Prepared for:

National Aeronautics and Space Administration
Goddard Space Flight Center
Greenbelt, Maryland 20771

Smithsonian Institution
Astrophysical Observatory
Cambridge, Massachusetts 02138

The Smithsonian Astrophysical Observatory
is a member of the
Harvard-Smithsonian Center for Astrophysics

The NASA Technical Officer for this grant is Ronald K. Oliversen, National Aeronautics and Space Administration, Goddard Space Flight Center, Greenbelt, Maryland 20771.

A Multi-Wavelength Study of the Hot Component of the Interstellar Medium

I. Goals

- Using the large number of lines of sight available in the IUE database, identify the lines of sight with high-velocity components in interstellar lines, from neutral species through Si VI, C IV, and N V.
- Compare the column density of the main components (i.e. low velocity components) of the interstellar lines with distance, galactic longitude and latitude, and galactic radial position. Derive statistics on the distribution of components in space (e.g. mean free path, mean column density of a component). Compare with model predictions for the column densities in the walls of old SNR bubbles and superbubbles, in evaporating cloud boundaries and in turbulent mixing layers.
- For the lines of sight associated with multiple high velocity, high ionization components, model the shock parameters for the associated superbubble and SNR to provide more accurate energy input information for hot phase models and galactic halo models. Thus far 49 lines of sight with at least one high velocity component to the C IV lines have been identified.
- Obtain higher resolution data for the lines of sight with high velocity components (and a few without) to further refine these models.

II. Summary

This research focuses on the kinematics and evolution of the hot phase of the interstellar medium in the Galaxy. The plan is to measure the UV spectra of all hot stars observed with IUE, in order to identify and measure the main component and any high velocity components to the interstellar lines. Data from higher resolution instruments will be collected for the interesting lines of sight.

IUE spectra of 240 stars up to 8 kpc in 2 quadrants of the galactic plane have been examined to (1) estimate the total column density per kpc as a function of direction and distance, and (2) to obtain a lower limit to the number of high velocity components to the interstellar lines, thus giving an approximation of the number of conductive interfaces encountered per line of sight. By determining an approximation to the number of components per unit distance we aim to derive statistics on interfaces between hot and cold gas in the Galaxy. We find that 20% of the stars in this sample show at least one high velocity component in the C IV interstellar line.

While it was expected that the number of high velocity components detected would increase with distance, assuming a uniform population of supernova remnants, single star bubbles, and superbubbles as well as tunnels or merged structures of hot gas, we find that high velocity features to the interstellar C IV line are generally confined to known supernova remnants and superbubbles, and there is no increase of the interfaces with distance in these 2 quadrants. Although the resolution of IUE of 10,000 is well below current instrumentation, the large number of statistics available with this dataset allow sampling many lines of sight with a photometrically stable detector and provide a guide for future investigation.

Two successful FUSE programs address this research and will collect data for several of the lines of sight identified as locations of hot, expanding gas. One program is complete for the Vela SNR. Another program to investigate the Cygnus superbubble is awaiting execution.

X-ray data from ROSAT, HST data, and Hα velocity data are being incorporated into the dataset.

Using the IUE and FUSE data, a detailed analysis of the shock structures in the Vela SNR has been conducted. An important result is that there is clear evidence that the shock front from the supernova has impacted multiple molecular clouds. This is providing an good example of realistic supernova remnant evolution in an inhomogeneous medium and its impact on the physical state of the interstellar medium. Using a Piecewise Parabolic Method

numerical hydrodynamics code to model the supernova remnant evolution, the evolution into a non-uniform, clumpy environment is being parameterized.

III. High-Velocity Gas in the Galactic Plane

Data Analysis

All IUE high dispersion spectra of O and B stars in or near the galactic plane (b=+/- 20 degrees) are being analyzed to identify and measure the main and any high velocity components to the interstellar lines. This class of stars was selected because of their strong UV continuum and, in general, lack of stellar features. Here the results of the C IV doublet analysis from 2 galactic quadrants, (2nd and 4th) are presented. The C IV doublet was chosen because it is most likely to indicate shock structures as opposed to H II regions, and to have accurate measurements of equivalent width (the N V is often absent or the continuum in this region has a complicated structure). The analysis includes measurement of the radial velocity of the components and the equivalent width. Only components with an equivalent width of more than 25 mA are considered, based on the resolution of the instrument, implying an upper limit to the detectable log N(C IV) of 12.8. Distances are from Hipparcus, if available. Otherwise, spectrophotometric distances were determined. Column densities have been calculated using a curve of growth analysis. Errors in the measurement of the equivalent widths range from 10% to 30% in most cases, although the errors can be as large as 100% when placement of the continuum was particularly difficult or the spectrum was unusually noisy.

Results

Figure 1 plots the distance of each star and the number of interstellar components detected in the IUE dataset for C IV. It is apparent that, at the resolution of IUE, the number of components do not increase with distance. Figures 2-5 plot the galactic position of each star and the symbols are color-coded to indicate the number of high-velocity components

detected in the spectrum of the star for C IV. These plots show that the high-velocity components are localized to specific lines of sight that can, in general, be linked to a SNR or OB association.

In spite of the rather low sensitivity of IUE compared with current instrumentation, the wealth of targets provides a large number of statistics that can be useful in identifying trends and placing upper limits on the column densities of shock interfaces in the galactic plane.

The fact that multiple components are generally confined to known SNR and OB associations suggests that interfaces between the hot and warm or cold phases of the galactic ISM are either few in number, aside from the known SNR and superbubbles, or have column densities below detectability with IUE. We will explore this issue by examining a few spectra of the more distant stars in our IUE sample from more sensitive instrumentation. The upper limit of column density for high velocity components constrains the theories of distribution and evolution of the hot phase of the ISM.

Figure 6 is a plot of the distance to the star vs. the C IV column density. Only stars for which the C IV doublet ratio is greater than 1.0 have been included. The mean density for the stars with d $\leq$ 3000 is 4.3 x 10^{-8}, an order of magnitude smaller than that found by Savage and Massa. This discrepancy could be due to a systematic difference in the method of measuring the equivalent width. Our larger sample of stars may also play a role. Also, we have used Hipparcus distances, which tend to be smaller than the spectrophotometric distances for this group of stars.

Figures 7 shows the number of interstellar line components in C IV as a function of C IV column density. No clear trend emerges here, contrary to our original concept that high velocity structures would tend to increase with length of the line of sight.

It was concluded that, at least for this limited dataset and the resolution of the IUE instrument, that high velocity gas is generally confined to known supernova remnants and superbubbles in the Galaxy. Other cooling interfaces of the hot phase of the ISM must have

radial velocities of less than 25 km/s relevant to the LSR, implying older structures. There are a few lines of sight that show high velocity C IV features that are not associated with known supernova remnants or OB associations.

Figure 1: Distance to the target stars (2nd and 4th galactic quadrants) vs. number of C IV interstellar components detected in the IUE spectra.

Figure 2: Position of the target stars in galactic coordinates for the 2nd galactic quadrant. Stars with spectra showing no high velocity components are indicated in black. Those with high velocity components are indicated in red. Note the clustering of the high velocity components in several regions.

Figure 3: Position of the target stars showing high velocity C IV components in galactic coordinates for the 2nd galactic quadrant. The number of high velocity components toward each star is indicated by the color.

Figure 4: Position of the target stars in galactic coordinates for the 4th quadrant. Stars with spectra showing no high velocity components are indicated in black. Those with high velocity components are indicated in red. Note the clustering of the high velocity components in several regions.

Figure 5: Position of the target stars showing high velocity C IV components in galactic coordinates for the 4th galactic quadrant. The number of high velocity components toward each star is indicated by the color.

Figure 6: Distance to the target stars vs. total C IV column density. The data have been fit for the complete sample, and also for those stars with distance less than 3000 pc, due to the scarcity of data at greater distances. The mean C IV density is indicated for both of these cases.

Figure 7: C IV total log column density plotted against number of components detected in the C IV line. Lines of sight with log column density greater than 15 have been identified as stars in supernova remnants and OB associations.

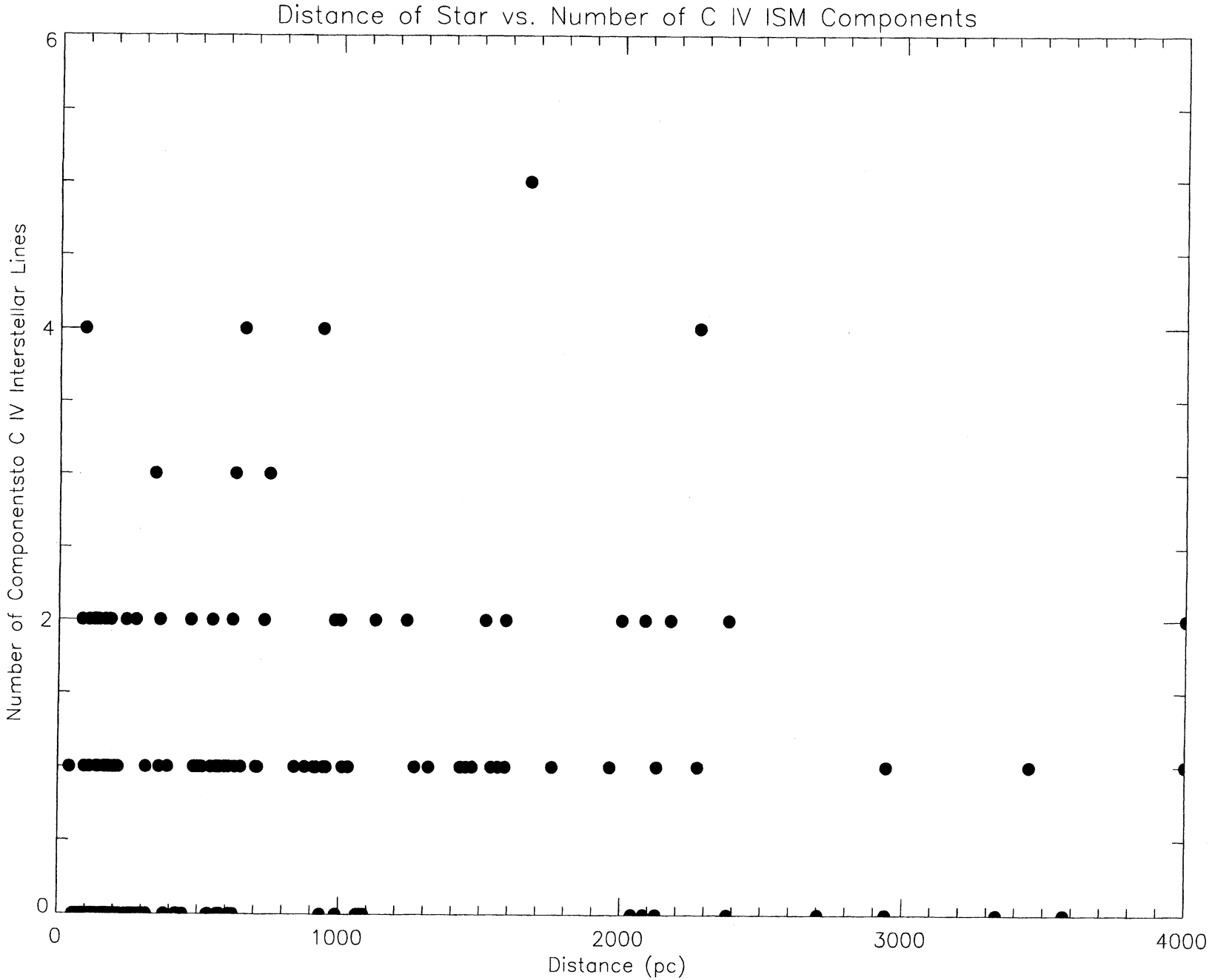
Distance of Star vs. Number of C IV ISM Components
Number of Componentsto C IV Interstellar Lines
Distance (pc)
0
2
4
6
0
1000
2000
3000
4000

FIGURE 1

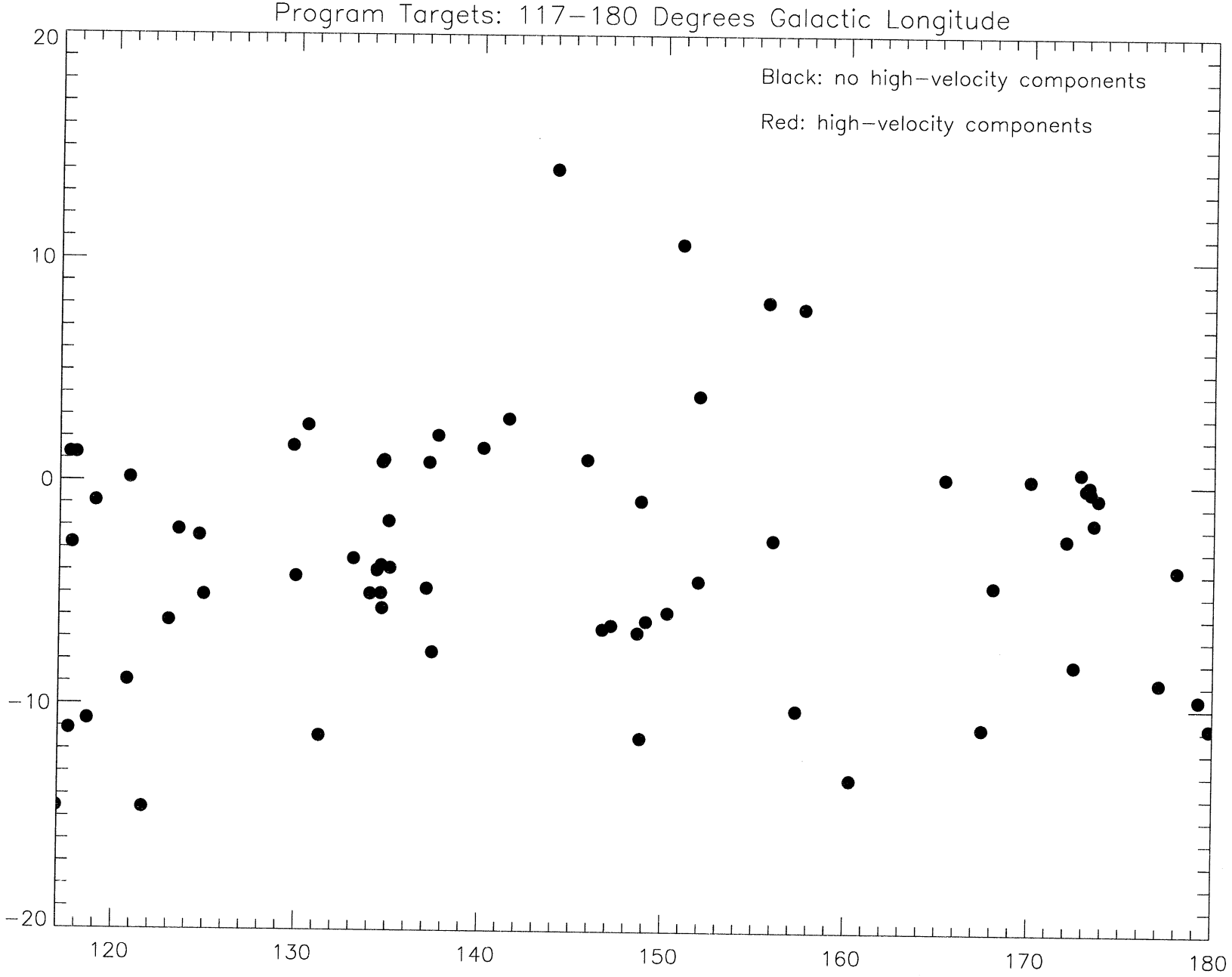
Program Targets: 117–180 Degrees Galactic Longitude
Black: no high–velocity components
Red: high–velocity components
20
10
0
−10
−20
120
130
140
150
160
170
180

FIGURE 2

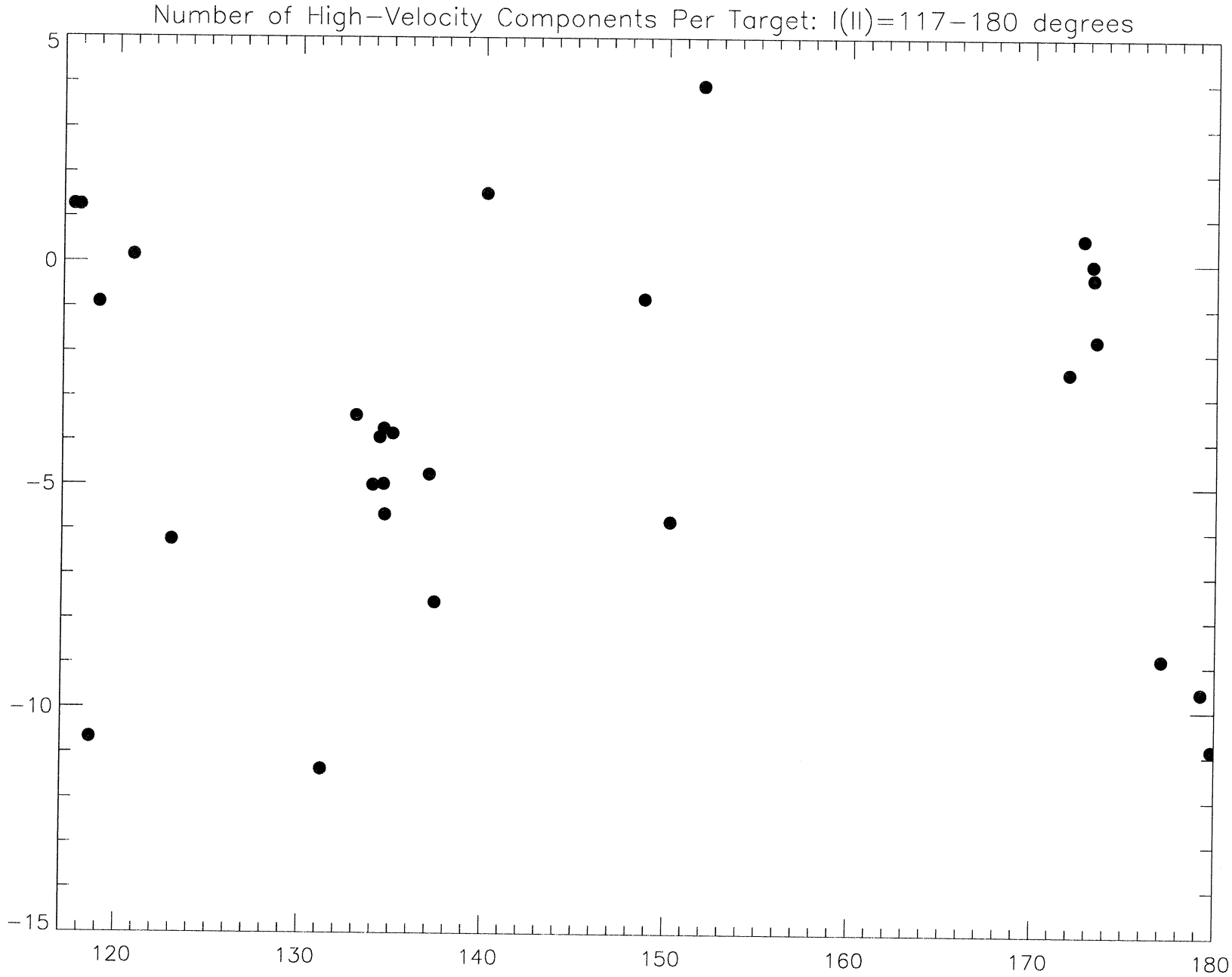
Number of High−Velocity Components Per Target: l(II)=117−180 degrees
5
0
−5
−10
−15
120
130
140
150
160
170
180

FIGURE 3

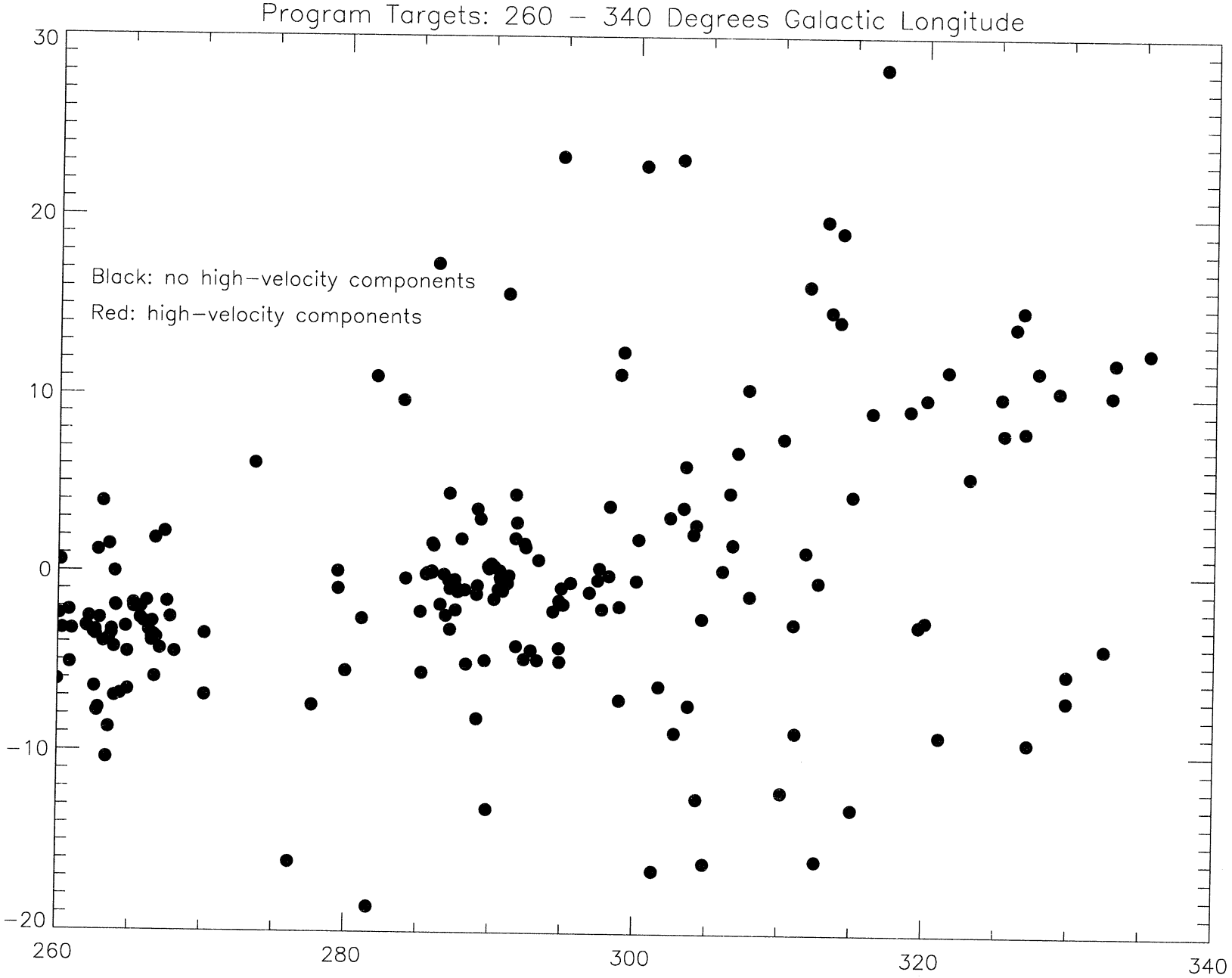
Program Targets: 260 – 340 Degrees Galactic Longitude
Black: no high–velocity components
Red: high–velocity components
30
20
10
0
−10
−20
260
280
300
320
340

FIGURE 4

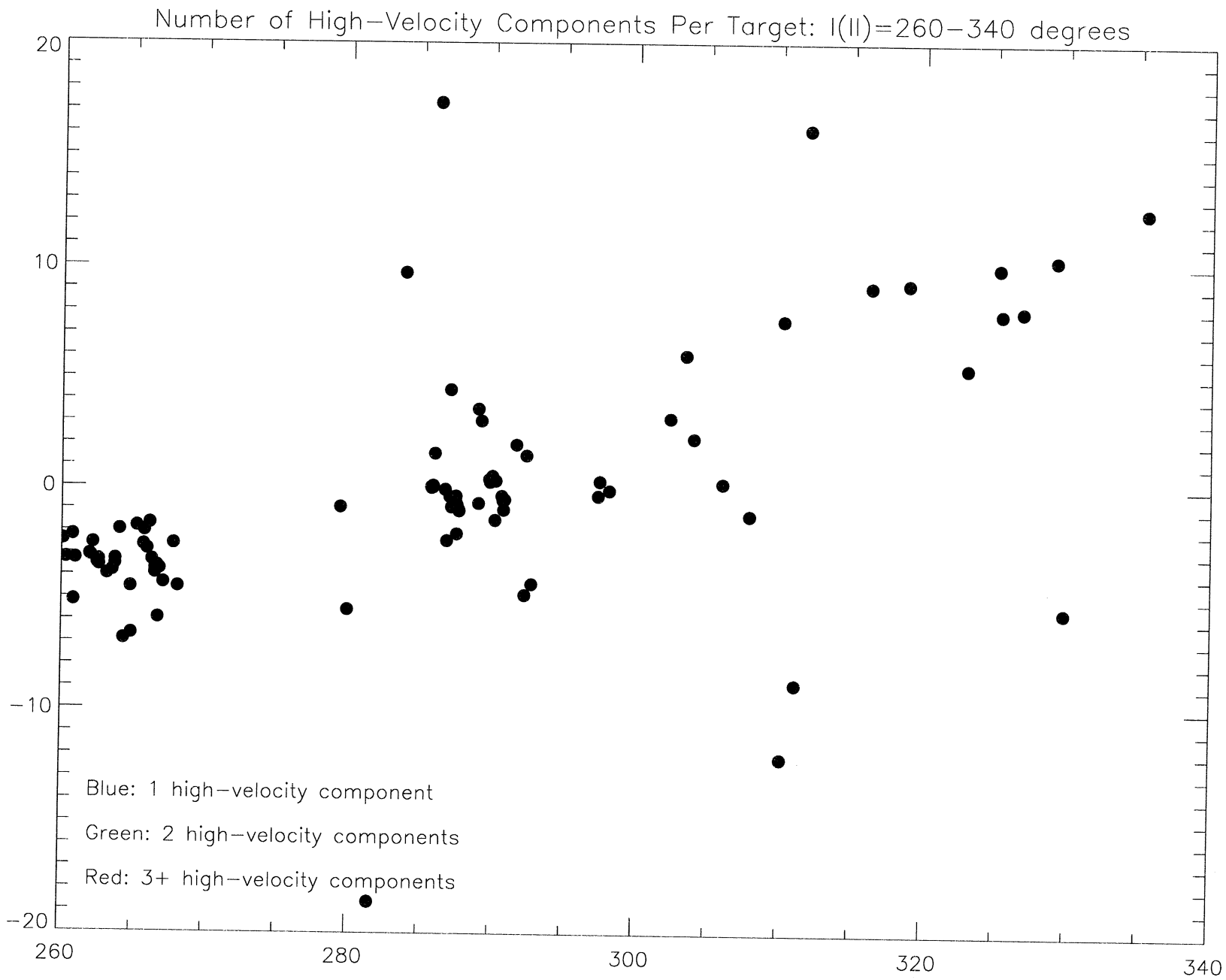
Number of High−Velocity Components Per Target: l(II)=260−340 degrees
20
10
0
−10
−20
260
280
300
320
340
Blue: 1 high−velocity component
Green: 2 high−velocity components
Red: 3+ high−velocity components

FIGURE 5

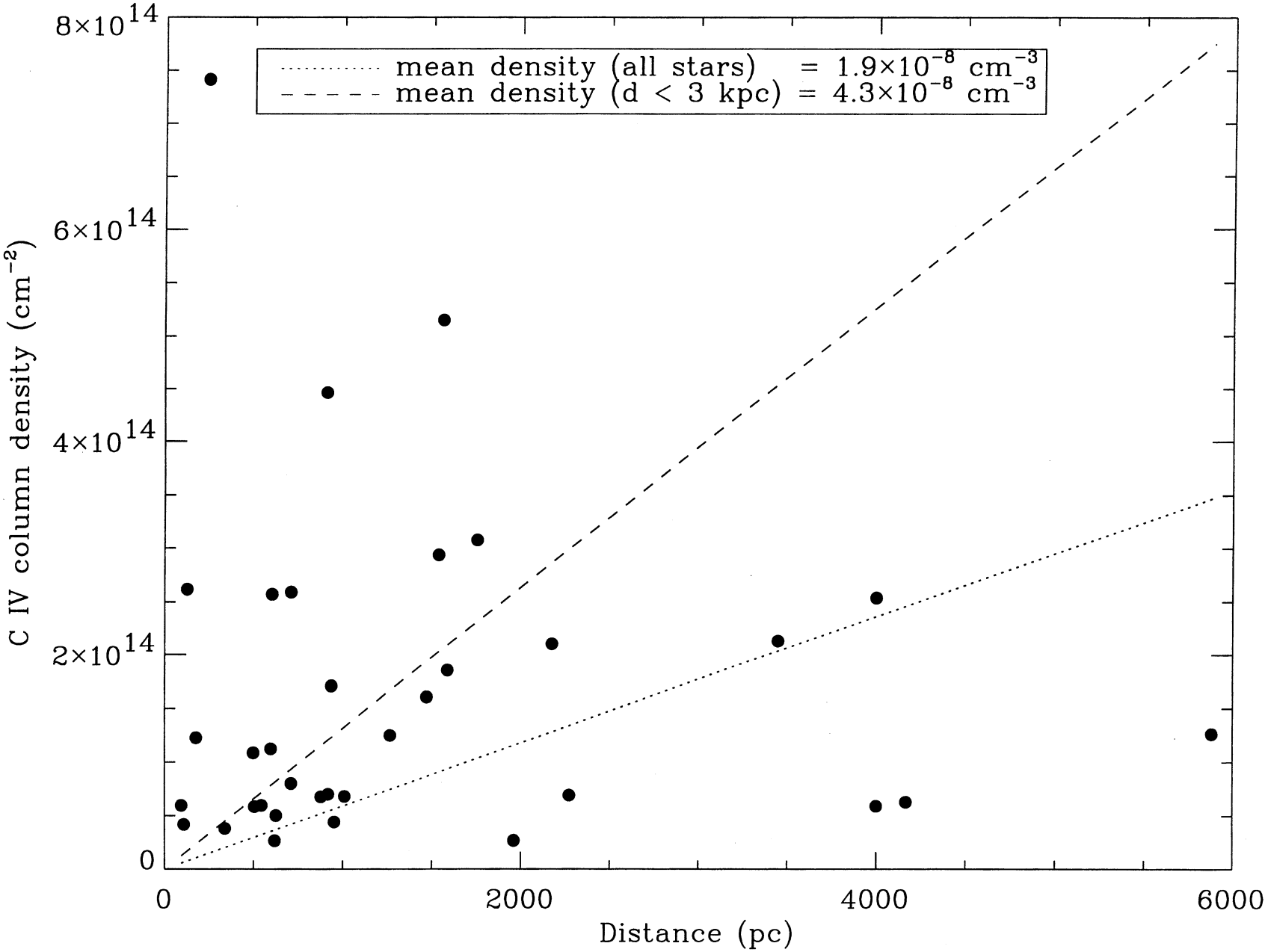
mean density (all stars) = 1.9×10^-8 cm^-3
mean density (d < 3 kpc) = 4.3×10^-8 cm^-3
C IV column density (cm^-2)
8×10^14
6×10^14
4×10^14
2×10^14
0
0
2000
4000
6000
Distance (pc)

FIGURE 6

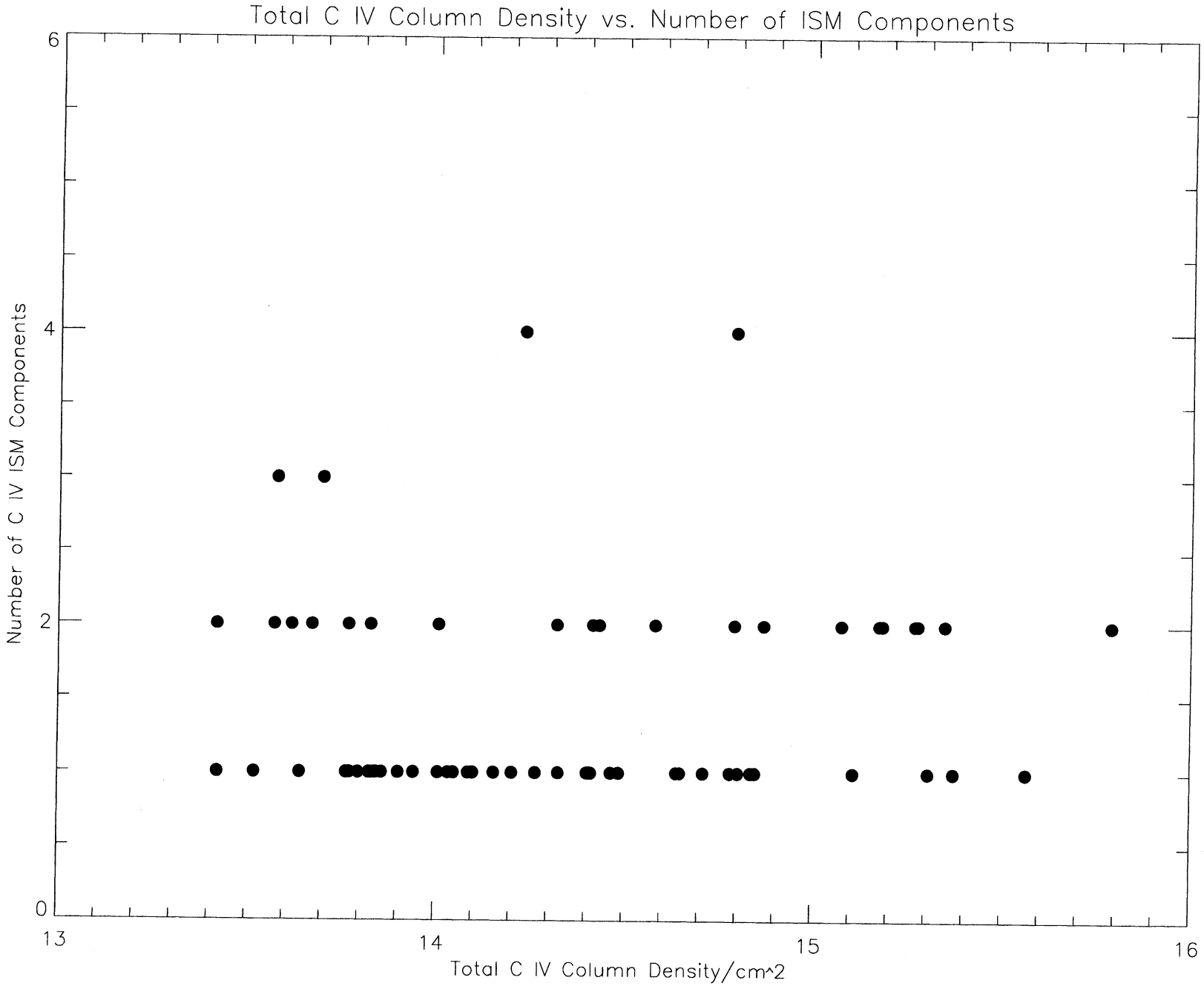
Total C IV Column Density vs. Number of ISM Components
Number of C IV ISM Components
0
2
4
6
13
14
15
16
Total C IV Column Density/cm^2

FIGURE 7

IV. High Velocity Gas in the Line of Sight to the Vela SNR

1. Introduction

One of the best objects for study of the structure, kinematics, and evolutionary status of a middle-aged supernova remnant (SNR) is the Vela SNR, due to its proximity (approximately 250 pc), extensive filamentary structure, and an abundance of hot background stars for absorption line research. The Vela remnant is 7.3° in diameter, based on x-ray imagery with ROSAT, with the pulsar nearly centered in the remnant (Achenbach et al. 1995). The western region of the remnant has much lower x-ray surface brightness than the remainder of the remnant and in fact escaped earlier detection with previous instrumentation.

Several studies of the interstellar absorption line data in optical wavelengths have previously shown the presence of high velocity features to the Ca II and Na I lines (Wallerstein & Silk 1971; Wallerstein, Silk, & Jenkins 1980; Jenkins, Wallerstein, & Silk 1984; Hobbs 1991; Danks & Sembach 1995; Cha & Sembach 2000), which can yield important information concerning gas kinematics, morphology, abundances and depletions, Even more remarkable that the numerous high velocity features recognized by these studies is the recent discovery that the interstellar features, including the high velocity features, are time variable with time scales of a few years (Hobbs 1991; Danks & Sembach 1995; Cha & Sembach).

High-velocity absorption components to the interstellar lines in ultraviolet data, which allow a much wider range of ionization potential and thus temperature, density, and pressure mapping, than are available in the optical wavelengths, were first reported by Jenkins, Silk, & Wallerstein (1976), who studied 4 stars in the Vela line of sight using Copernicus data. They found velocities in the range of –90 km s^{-1} to +180 km s^{-1} with a possible component at –450 km s^{-1}. Jenkins, Wallerstein, & Silk (1984) studied absorption line profiles in IUE high dispersion data of 45 stars in the Vela line of sight, finding high velocity components in more that one third of the program stars, with velocities up to +180 km s^{-1}. Their analysis of IUE data showed chaotic kinematics, no geometric effects of expansion, lower depletion

than the normal interstellar medium (ISM), and some relatively strong lines of C I. Raymond, Wallerstein, & Balick found evidence of a thermally unstable shock wave behind a 150 km s^{-1} shock. Their calculations also indicate the shock is nearly face-on. An important result by Jenkins & Wallerstein (1995) revealed 6 distinct high-velocity components to the interstellar C I lines for one star behind Vela, HD 72089, using GHRS data. These authors conclude the +121 km s^{-1} component represents gas that has cooled and recombined behind the shock wave. They also find that the implied energy of the supernova is too large if a distance of 500 pcs is accepted. They proposed instead a distance of 250 pc. Their conclusions were later confirmed and extended with STIS (Jenkins et al. 1998).

This paper describes the absorption line analysis of IUE data of 60 stars in the Vela SNR region. While IUE high resolution data do not have the resolution of more current instrumentation, the large number of spectra available in the IUE archives provide an opportunity to map spatially the high-velocity components to the interstellar lines and compare the morphology of the hot gas to X-ray imagery. The IUE archive has been reprocessed with improved calibrations and image processing techniques, so that revisiting previously published results of earlier investigators is useful because of the reduced errors and comparablity of the spectra.

2. Observations

We are currently engaged in a survey of all high disperion IUE data of hot stars near the galactic plane with the goal of cataloging high-velocity components in the interstellar absorption lines. The project includes high ionization (C IV, Si IV, and N V) and low ionization (Fe II, C II, Si II, Al II, and S II) lines present in either SWP or LWP/R spectra of O and B stars. We have selected all stars in the IUE archive with $258° \leq l_{II} \leq 269°$ and $-8° \leq b_{II} \leq +2°$ for study of the Vela SNR. These stars are listed in Table 1, along with their galactic coordinates, Hipparcus distance estimates, spectral types, and IUE image sequence numbers analyzed. While the sampling of the region is generally quite good, there are a few unsampled pockets evident in the figure, particularly about 1° west and 1° east of the Vela

pulsar. The lack of data in these regions must be considered in the conclusions to this work. The spectra used in this survey were processed with NEWSIPS.

These spectra were corrected to heliocentric velocities in the NEWSIPS processing. Even after correction to heliocentric velocities, there are residual errors in each spectrum due to image distortion and spectra format motion. We would have preferred to add a correction to each radial velocity measurement which was determined from the mean of the neutral ion lines as has been done in previous studies (Nichols-Bohlin & Fesen, 1986, 1993), but as noted below, the neutral C I (the majority of the available neutral ions in SWP spectra) are variable and sometimes have high-velocity components of their own, making them unreliable fiducials in the Vela region. We therefore report heliocentric velocities assigned in the NEWSIPS processing. There is one remaining important source of error in the radial velocities reported here. The long-wavelength spectrum of an object often has a velocity offset from te SWP spectrum of the same object, based on the mean of the main interstellar components and in particular on the Fe II λ1608 line radial velocity in the SWP spectrum compared to the Fe II λ2382, 2585, 2599 lines in the LWR/P spectrum. This offset, which is generally about $+17$ km s^{-1} for the LWR/P spectra, has been previously reported (Nichols-Bohlin & Fesen 1986) but the source of the error remains unknown. Because the error is not always present, and SWP spectra analyzed here form a consistent group of main component velocities, we assume the error is in the long-wavelength assignments from IUESIPS, and have corrected these velocities such that the main components in the LWP/R spectrum match those in the corresponding SWP spectrum.

Another source of uncertainty in this study is the non-uniform time epoch. As Cha & Sembach (2000) have shown, the velocities and the equivalent widths of the interstellar line components in this region can vary of time scales of a few years (or less). While most of the spectra used in this study were taken during 1978-1979, a few were taken as late of the mid-1990's.

It was not always possible to measure all of the interstellar absorption lines. For exam-

ple, the C II line at 1334 Å is contaminated by a reseau mark in large aperture spectra, discounting valid measurements. Al II lies at the end of an echelle order and the ripple correction for this order can be unsatisfactory, producing spurious features. Al III has not been included in this study because it almost always includes a photospheric component for the spectral type of the stars in this study. The data for Si II presented in the following tables include a summary of 4 lines (1260 Å, 1304 Å, 1506 Å, 1808 Å). Although the Si II lines at 1190 Å and 1993 Å were always examined, this region of the IUE echellogram is almost always too noisy to make confident measurement. The main component, not reported in the tables, generally lies at +7 - +17 km s^{-1} in the Vela direction.

The equivalent width of each high velocity feature was measured using an interactive tool provided by the IUEDAC. Two points on either side of the feature were selected to represent the continuum. These points were selected in regions at least .5 Å from the edge of the feature being measured, in a region devoid of any identifiable absorption or emission features. If it were assumed that the data represent the true continuum with no absorption or emission features, then the appropriate continuum level would lie halfway between the maximum and minimum flux values that represent the noise in the data. Since it is assumed there are still unidentified absorption features below the resolution of IUE, the continuum was chosen as approximately 0.75(maximum data value - minimum data value) + minimum data value. The equivalent width is the total area below the selected continuum. The radial velocity of the line is represented here as the minimum extremum in the line center. This is not as accurate as a gaussian fitting technique, and the errors reflect the reduced accuracy. The intent of this work was to identify lines of sight that warrented future investigation, and gain a global view of the ionization and kinematics in the various lines of sight toward the Vela SNR.

The high-velocity C I features presented here represent a serendipitous discovery which occurred while surveying the spectra of stars in the line of sight to the Vela SNR. Because the wavelength assignments in high dispersion data are not sufficiently reliable to be used

directly for absolute velocity displacements of high- velocity features, we normally measure the radial velocity of a series of neutral features (C I, Cl I, Si I) in each SWP image and use the mean of these velocities to determine the heliocentric radial velocity of high-velocity features found in each spectrum. However, in making the C I measurements, we found that many stars had displaced C I lines with respect to the main components of the other interstellar lines in the spectrum, and eleven stars actually showed high-velocity features in the C I lines, with the high-velocity feature of similar strength to the main component. Because the intent of our investigation was to measure the low and high ionization lines for high-velocity features, and to use the C I lines as fiducials, no equivalent widths were measured. The number of stars showing high-velocity C I presented here must be considered a lower limit, because high-velocity components were recorded only when they were equal to or greater strength compared to the main component. Indeed, it was only at the conclusion of our study of the Vela region that the consistent pattern of high-velocity C I in this region was recognized.

The target stars have been separated into 7 spatial groups for ease of discussion. Regions 1-5 are arcs of the circular supernova structure, inside the X-ray contours, and are numbered clockwise around the the remnant beginning in the northwest at the line of sight to Pup A. There is also an "M" region for the center of the supernova remnant, and an "O" region for stars outside the projected X-ray contour.

3. Discussion

3.1 Neutral Species Discussion

Table 2 lists the HD numbers of the eleven stars which show high-velcity C I in SWP IUE spectra and Mg I in LWP(R) spectra, distance estimate, and displacements velocities of the high-velocity components. These stars are generally confined to a band extending from the north edge (near Pup A) to the south edge of the X-ray image. This band is about 1° wide on the image. This clearly defined spatial morphology of this region of high-velocity C

I implies the high-velcity gas arises from a single coherent structure. The structure is most likely associated with the Vela SNR because (1) there is a lack of such high-velocity C I gas outside the x-ray region except for 1 star slightly outside the south-west edge of the remnant and not associated with the "band" in the interior of the remnant, and (2) the velocity is consistent with the most pervasive high-velocity components in other species detected toward Vela. The fact that all of the high-velocity components have positive velocities is particularly helpful in determining the nature of the associated high-veloctiy gas. The band must be on the back side of the remnant only and confined to a small region, suggesting it is not pervasive in the supernova shell but perhaps a dense, pre- existing cloud in the ISM which is now interacting with the SNR. The band of high- velocity C I lies close to the sharp line in the ROSAT x-ray image separating the high surface brightness region (previously seen by EINSTEIN) and the low surface brightness region, newly revealed with ROSAT. However, the high-velocity C I structure lies inside the high surface brightness region.

3.2 Low Ionization Discussion

The stars exhibiting high velocity features in low ionization lines are listed in Table 3 along with the velocity displacement for each of the singly ionized species. While it is clear from these data that the lines of sight intersect multiple cooling regions, it is also clear that these regions are quite patchy and stars separated by as little as 1 pc show different velocity structures.

There is a concentration of components at -90 km s^{-1} and +120 km s^{-1}. Also, there are two stars with a component at +400 km s^{-1} and two stars with a component at +500 km s^{-1}. There are also apparent components at +150 km s^{-1} and -140 km s^{-1}. The occurance of these features appears to be random across the Vela SNR in the region sampled by the program stars and geometric effects are not clearly evident, although they may be present in the components with radial velocity $\leq$ 100 km s^{-1} seen in a number of the stars. However, these lower velocity components are not confined to the outer regions of the Vela

remnant and cannot be exclusively attributed to the lower velocities expected when viewing the edge of a shell as opposed to the center. These lower velocities may indeed represent an additional structure to the obvious one at v = 100-120 km s^{-1} and v = 400-500 km s^{-1}.

3.3 Si IV Discussion

There are far fewer high-velocity components to the Si IV lines (total of 19 in our sample) than are present in either the low ionization lines (39 in our sample) or in the C IV data (56 in our sample). The smaller number of components compared to the low ionization lines may be understandable since there are 7 low ionizaton lines normally measured in each spectrum as opposed to two Si IV lines (a doublet). The components at -100 km s^{-1} and +120 km s^{-1} are again the most common, with the +150 km s^{-1} components also well represented. In addition, two components are present at -225 to -250 km s^{-1} and two components at -800 km s^{-1}. There is one component at -420 km s^{-1} and one at -350 km s^{-1}. While components present in only one spectrum are viewed as questionable, these two components have counterparts in the low ionization data (-400 km s^{-1}) and in the C IV data (-350 km s^{-1}).

3.4 C IV Discussion

The C IV high-velocity features are remarkable for their high frequency of incidence, especially considering that only 2 lines per spectrum contribute to the statistics. As in the cases of the low ionization lines and the Si IV lines, the -100 km s^{-1} and +120 km s^{-1} components dominate the statistics, with the +150 km s^{-1}also well represented. Here we see the strongest evidence for additional high-velocity structures. The v = +400 km s^{-1} components are clearly identifiable as a distinct structure, with 4 stars showing this component. The component at -325 km $s^{-1}$to -350 km $s^{-1}$is also well defined, with 4 stars exhibiting these components. This set of components, like the [-100,+120] set, indicate a shell of cooling material expanding in Vela about the systematic velocity of +20 - +30 km s^{-1}, although, again, no geometric efects are clearly seen. There are also components at -230 km s^{-1} and

+350 km s^{-1}, which may be statistically significant.

4.0 General Discussion

4.1 Distance

This study supports the proposal by Jenkins (1995) that the distance to Vela should be revised. The distance of 400-500 pc has been accepted, primarily because of the presumed association between Vela and the Gum Nebula. Jenkins suggested that Vela is at 250 pc due to energy considerations. Two the the stars in this study which show positive C I components have distance estimates of 320 and 360 pc, respectively. In addition to C I, these 2 stars show positive velocity components in both low and high ionization lines, most of which are positive velocity components. Thus, a revised distance of 200-300 pc for Vela SNR would be consistent with our data. We note Ashenbach (1998) also suggested a revised distance for Vela of 250-350 pc.

4.2 Global Mapping

Because our coverage of the Vela region is not complete, it is difficult to describe the morphology of the structures responsible for the high-velocity gas. We can certainly conclude that the structures are patchy because detection at IUE's resolution varies over distances as short as a few parsecs. The structures do not appear to be shells expanding uniformly from the center of Vela due to the lack of geometric effects, which leads us to conclude that these are preexisting clouds overrun by multiple shocks.

Considering the distances of the stars studies, we find the various high- velocity components may originate in spatially distinct regions. For stars with distance estimates less than 580 pc, only the -90, +120, and +150 km s^{-1} components are seen in any ionization state. The +400 and +500 km s^{-1} components appear in stars with distance estimate $\geq$ 580 pc. This would imply that the higher velocity components are formed in a different, background structure to the lower velocity components. The Gum Nebula and the Vela SNR are at

similar distances and it is concievable that some of the high-velocity components arise in the Gum Nebula rather than the Vela SNR. However, we find no evidence for such high-velocity components in stars outside the Vela region. The distance differentiation could be fortuitous, because the higher velocity components are few in number. Assuming the –90, +120, and +150 km s^{-1} components are associated with the Vela SNR, we estimate the distance to the Vela SNR to be 300-350 pc, based on the positive velocity components in HD 70930 at 375 pc.

The distribution of high-velocity components suggests the most prevalent components (–90, +120, +150 km s^{-1}) are global in the Vela SNR and perhaps associated with the cooling interface behind the shock wave of the supernova. The higher velocity components (+400, +500 km s^{-1}) are less uniformly distributed but still cover the entire projected SNR. It is difficult to believe that these components arise at the conductive interface of several clouds embedded within the SNR because of the consistent velocities at several lines of sight to the SNR. Other components occurring in more localized regions could be interpreted as conductive cloud interfaces. Danks & Sembach (1995) suggest that some of the high-velocity gas in Vela may be accelerated by events other than the Vela SNR, based on the wealth of components seen in the spectra of member stars of IC2395, situated in the line of sight to the southeastern edge of the Vela X-ray perimeter. This is a somewhat confusing result because if the high- velocity features arise in the cooling gas behind the supernova shock wave, the velocities in this region should be near zero, yet the velocities are consistent with those seen near the center of the remnant. This situation prompted Danks & Sembach to suggest that some of the high-velocity gas in Vela may be due to events other than the original supernova. We agree with their suggestion and find that the velocity structure we have mapped can be reasonably explained if at least one other explosive site is considered.

4.2 Neutral High-velocity Gas

An important finding of this study is that multiple lines of sight toward the Vela SNR exhibit high velocity interstellar components in the neutral lines of C and Mg. The stars

that show such high velocity neutral components in their spectra are spatially related in that they form a "ridge" running north to south along, but inside of, the western rim of the x-ray bright SNR. The detection of such high velocity neutral gas is quite unusual. The examination of hundreds of IUE spectra of hot stars in the galactic plane has not revealed another occurrance of this phenomenon, at the resolution of IUE. Neutral C quickly combines in molecular clouds to become CO, and virtually no C I would be expected in a molecular cloud. On the surface of a molecular cloud, interaction with a shock front could create conditions in which C I is formed and remains stable for a period of time. Our data suggest that the western portion of the Vela SNR is impacting or engulfing an molecular cloud, accelerating the cloud to high velocity.

There is strong evidence that a molecular cloud, or more likely a group of clouds, encase the Vela SNR on the back side. The optical filamentary structure seen toward the SNR is presumably formed at the surface of molecular clouds as they interact with a shock. The fact that we clearly see this filamentary structure indicates it is formed on the side of the molecular clouds facing us, and that therefore the molecular cloud(s) are on the far side of the remnant and receding. This view is supported by our data that the C I high velocity features are all positive.

In particular, a CO cloud is clearly identified by Moriguchi et al. (2001) at l_{II}=262.4° , b_{II}=-3.4° . This cloud is correlated with a region of optical filaments and includes the lines of sight to 7 stars, which show positive high velocity C I.

The four C I lines examined in our analysis are each the ground state transition in multiplets of up to 5 transitions. Each group of lines is generally too complicated to measure any but the strongest component at the resolution of IUE. This situation also leads to lower reliability of measurements. However, each of the 4 multiplets has a different set of components transitions, so that strong features verified in most of the multiplets can be considered reliable. Occasionally, the wavelength region of a multiplet was too confused to measure any component.

Jenkins observed HD 72089 with HST, measuring the components of the C I lines 1656Å, 1329Å, and 1280Å. They find evidence of 6 high-velocity components in the line of sight ot HD 72089, which lies only a few parsecs, a star in our study, and also well within the band of stars showing high-velcity C I in our study. We did not detect high-velcotiy C I for HD 72089 in the IUE data because the high-velcity features are not as strong as the main component in the ground star C I and the high-velocity feature at +121.5km s^{-1} is blended with other lines in the multiplet at IUE's resolution. As mentioned above, we were not looking specifically for high-velcity features in C I. This illustrates the fact that the number of stars showing high-velcity C I listed in Table 3 is a lower limit.

Certainly, the clear detection of positive velocity C I in the HST spectrum of a star along nearly the same line of sight as many of the stars we studied validates the IUE results. Jenkins' analysis of the high-velocity neutral and excited star C I indicates the gas producing the high-veloctiy C I absoption features in UV data is in a high density and high pressure zone behind the shock front that has cooled and recombined.

The detailed analysis and conclusions of Jenkins in reference to the neutral and excited state C I gas in the Vela SNR appear to be generalizable to the band of high-velocity neutral gas described here. It is posssible that the high pressure and density region is not a distinct cloud or structure in the SNR, but is global to the SNR in the sense that a shell of neutral recombined gas exists in the post shock material, with the column densities large enough to be detected with IUE only in the western limb. But in this case, some negative velocity components should probably have been detected. The data suggest we are viewing evidence of pre-supernova inhomogenieties in the ISM. The sudden drop in x-ray surface brightness to the west of the band of high pressure, high-velocity gas implies high N_H.

Conclusions

1. High velocity C I present in several lines of sight toward the western portion of the Vela SNR indicate molecular cloud/shock interactions in this region. Combined with the

numerous optical filaments in this line of sight, one can conclude that the SNR has interacted with many small molecular clouds (possibly engulfing some of them) or a large molecular cloud that is pervasive on the backside of the remnant.

2. The presence of multiple high velocity components in many lines of sight to the Vela SNR indicate multiple shock structures and a complex environment.

3. The Vela SNR is expanding into a non-uniform environment that appears to have molecular clouds nearby and quite possibly radically different ambient densities on the front and the back side of the remnant.

4. The expansion velocities determined for the various components are not consistent with a geometrically expanding shell. The data are more consistent with multiple explosion sites, with the possibility of multiple supernovae.

5. The broad range of ionization species and column densities seen in the various lines of sight toward Vela suggest significant temperature variations and well as shock speeds in this supernova.

References

Ashenbach, B., Egger, R., & Trumper, J. 1995, Nature, 373, 587.

Aschenbach, B. 1998, Nature, 396, 141.

Cha, A. N. & Sembach, K. R. 2000, ApJS, 126, 399.

Cha, A. N., Sahu, M. S., Moos, H. W., & Blaauw, A. 2000, ApJS,

Danks, A. & Sembach, K. 1998, AJ, 109,2627.

Hobbs, L. M., Ferlet, R., Welty, D. E., & Wallerstein, G. 1991, ApJ, 378, 586.

Jenkins, E. B., Silk, J., Wallerstein, G., & Leep, M. 1981, ApJ, 248, 997.

Jenkins, E. B., Wallerstein, G., & Silk, J. 1984, ApJ 278, 649.

Jenkins, E. B. & Wallerstein, G. 1995, ApJ, 440, 227.

Jenkins, E. B., Tripp, T. M., Fitzpatrick, E. L., Lindler, D., Danks, A. C., Bech, T. L., Bowers, C. W., Joseph, C. L., Kaiser, M. E., Kimble, R. A., Kraemer, S. B., Robinson, R. D., Timothy, J. G., Valenti, F. A., & Woodgate, B. E. 1998, ApJL, 492, L147.

Moriguchi, Y., Yamaguchi, N., Onishi, T., Mizuno, A., & Fukui, Y. 2001, PASJ, 53, 1025.

Nichols-Bohlin, J. & Fesen, R. A. 1993, AJ, 105, 672

Nichols-Bohlin, J. & Fesen, R. A. 1986, AJ, 92, 642.

Wallerstein, G., & Silk, J. 1971, ApJ, 170, 289.

Wallerstein, G., Silk, J., & Jenkins, E. B. 1980, ApJ, 240, 834.

Table 1. Stars Observed in the Vela SNR Region

Star	lII	b II	Spec. Type	distance	SWP	LWP(R)
AL Vel	265.07	-4.91	K0 III + A3 IV		33974	23459
HD 68217	260.07	-5.96	B2 IV/V	348.432		17597(R)
HD 68243	262.81	-7.70	B1 IV		32408	12177
HD 68273	262.80	-7.69	WC	257.732	43022	04753(R)
HD 69404	262.58	-6.46	B2 Vnn	408.162	05534	04791(R)
HD 69648	260.88	-5.10	O+		25707	05769
HD 69882	259.50	-3.91	B1/B2 Iab/Ib	7142.86		05524
HD 69973	264.01	-6.90	B4 V	416.667	05511	
HD 70084	263.38	-6.34	B5 II/III	389.105	20860	
HD 70309	264.41	-6.81	B3 III	252.525	05530	
HD 70930	264.98	-6.50	B1 V	462.963	05531	
HD 71019	260.37	-3.14	B3 II/III		09434	05523
HD 71216	258.81	-1.78	B5 Vnn	440.529	20191	16127(R)
HD 71336	261.01	-3.21	B3 III/IV		09433	
HD 71459	260.10	-2.40	B3 V	249.377	05533	04790(R)
HD 72014	260.77	-2.20	B1/B2 V:nne	925.926	05495	04763(R)
HD 72067	262.08	-3.08	B2 Vne	490.196	29376	
HD 72088	262.67	-3.49	B3 III/IV		38714	17847
HD 72089	263.21	-3.89	B5 II/III		14096	10734(R)
HD 72127A	262.57	-3.36	B3 III		43030	21659
HD 72179	262.08	-2.97	B4 II/III		14117	05739
HD 72230	262.63	-3.31	B9 V		14118	
HD 72232	263.91	-4.26	B5 III	193.050		10738(R)
HD 72350	262.71	-3.19	B4 IV	684.932	44774	21662
HD 72537	263.65	-3.67	B3 V	377.358	05529	
HD 72555	264.84	-4.53	B2 V	393.701	05555	
HD 72648	262.23	-2.48	B1/B2 Ib	740.741	14126	
HD 72754	266.83	-5.82	B2 Ia:pshe	689.655	05888	05143(R)
HD 72798	263.77	-3.46	B3 III	751.880	14102	10737(R)
HD 72997	262.92	-2.58	B2 II/III	621.118	05549	
HD 73010	263.80	-3.23	B5 V	746.269	05550	

Table 1 (con't). Stars Observed in the Vela SNR Region

Star	lII	b II	Spec. Type	distance	SWP	LWP(R)
HD 73658	264.68	-3.13	B1 Ib/II	719.424		
HD 73882	260.18	+0.64	O9 III	500.	38311	11718(R)
HD 74194	264.04	-1.95	O+	2777.78	05527	
HD 74234	266.56	-3.87	B2 IV	628.931	05491	10735(R)
HD 74273	267.13	-4.27	B1.5 V	429.611	05494	
HD 74319	264.07	-1.80	B3 V	401.606	05505	10736(R)
HD 74371	264.44	-2.01	B6 Iae	826.446		16708
HD 74436	266.70	-3.72	B3 V	411.523	05525	
HD 74530	266.62	-3.55	B3 IV/V		05487	
HD 74531	266.68	-3.61	B2 V:	775.194		04759(R)
HD 74580	266.69	-3.55	B3 V		05488	
HD 74620	266.36	-3.25	B4		05504	
HD 74662	266.90	-3.63	B3 V		05526	
HD 74711	265.73	-2.61	B2 III		14125	
HD 74753	268.11	-4.49	B0 IIIn	465.116	05557	04799(R)
HD 74773	266.02	-2.76	B3 IV	840.336	05553	
HD 74920	265.29	-1.95			05559	
HD 75129	266.59	-2.74	B5 Ib	502.513	14123	
HD 75149	265.33	-1.69	B3 Ia	1010.1	07726	
HD 75309	265.86	-1.90	B2 Ib/II		14124	
HD 75549	263.86	+0.01	B3 V	330.033	14104	
HD 75759	262.80	+1.25	B1.5 III	584.795	06397	22403
HD 75821	266.25	-1.54	B0 III	826.446	05560	08012
HD 76161	267.89	-2.43	B3 Vn	333.333	06635	10751(R)
HD 76341	263.51	+1.52	O9 I	1219.51	28157	06999
HD 76534	264.42	+1.05	B2 Vn		47830	25704
HD 76536	267.55	-1.64	WC	3448.28	10113	
HD 76566	265.64	+0.05	B3 IV	286.533	14121	10750(R)
HD 78616	266.79	+1.97	B2 II/III	1250.00	10804	

Table 2. Stars Showing High-Velocity Neutral Species in their IUE Spectra

Star	Region	distance	C I velocity	Mg velocity
HD 71549	1	249	+111	
HD 71336	1		+116	
HD 72014	1	925	+116	
HD 72648	1	740	+97	
HD 72127	1	2127	+73	
HD 72350	1	684	+106	
HD 72088	1		+86	
HD 72535	1	393	+98	
HD 72179	1			+96
HD 72089	1			+104
HD 74662	2		+94	
HD 72537	2	377	+93	
HD 75821	M			-65
HD 76161	M			+88
HD 76534	4			-58
HD 70309	5	252	+98	

Table 3. Region 1 Stars Showing High Velocity Low Ionization Components

Star	Si II 1260	Si II 1304	Si II 1526	Si II 1808	C II 1334	C II 1335	Al II
HD 71216	-52	-59	-52	-63	-64	-52	-50
HD 71459	(+164)	(+154)	(+88)		(+884)	(+856)	
HD 71019							
HD 72014					-63	-67	
HD 71336						+89	
HD 72179			+157		+152	+87,+142,+418	
HD 72067			(-81)				
HD 72648						-10	
HD 72127			+128			-1	
HD 72350	+7,+102,+294		+128	-42			-95,-44,+158
HD 72088			-45,0,+92,+155		-45,+86,+126	-55,-10,+4,+126	
HD 72089		+120	-42,+114		+130	+122	+119

Table 3. Region 1 Stars Showing High Velocity Low Ionization Components

Star	Fe II 1608	Fe II 2382	Fe II 2585	Fe II 2599	Mg II 2795	Mg II 2802	Mn II 2576	Mn II 2593	N
HD 71216		-26		-23		-27	-30		
HD 71459							(+144)		
HD 71019	-140	+206			+10, +62	+11, +47			
HD 72179		+94	+96	+96,+149,-110,(+486)	+512	+520			
HD 72127				+110			+67		
HD 72350	-126		+147	+149	-104,+116,+153	-97,+121,+154			
HD 72088	-42,-18	-33,-2,+49	-27,+48	+9,+43	-32,+7,+59,+151	-21,+14,+54,+127	-9		
HD 72089	+88	-60,+104	+111	-53,+104	-49,+104	-46,+101			

Table 3. Region 2 Stars Showing High Velocity Low Ionization Components

Star	Si II 1260	Si II 1304	Si II 1526	Si II 1808	C II 1334	C II 1335	Al II
HD 74530	(-85)	-278,-187,(-76)		-169,-84	-111		
HD 74580	-87	-90	-80		-106	(-132),(-69)	-76
HD 72754			+126+				

Table 3. Region 2 Stars Showing High Velocity Low Ionization Components

Star	Fe II 1608	Fe II 2382	Fe II 2585	Fe II 2599	Mg II 2795	Mg II 2802	Mn II 2576	Mn II 2593	Mn II 2605
HD 74234		+80	-40	+65	+70	+71			
HD 74531		-172		(-181),-132	-140				-139
HD 74580	+67								
HD 72754			+70		-1183	-1177			

Table 3. Region 3 Stars Showing High Velocity Low Ionization Components

Star	Si II 1260	Si II 1304	Si II 1526	Si II 1808	C II 1334	C II 1335	Al II
HD 75149	c	c	+124		c	c	
HD 76566		(-125),(+132)	+107			-90	
HD 74711	-100				+121		
HD 75309	-61	(-110)	-63	(-39)	-237,-24,+197,+399	+241,+395	
HD 75821	+99,(-75)	-82	-73,+101		-71,+122	-70,+126	-60

Table 3. Region 3 Stars Showing High Velocity Low Ionization Components

Star	Fe II 1608	Fe II 2382	Fe II 2585	Fe II 2599	Mg II 2795	Mg II 2802	Mn II 2576	Mn II 2593	Mn II 2605
HD 76566	(-117)		-103	-84	-146				
HD 75821		-61,+100	-63	-64	-66,+108	-70,+105			

Table 3. Region 4 Stars Showing High Velocity Low Ionization Components

Star	Si II 1260	Si II 1304	Si II 1526	Si II 1808	C II 1334	C II 1335	Al II
HD 75759	-6	+5	+10		-10,+100	-6,+102	
HD 76341	-5	-13				-5	

Table 3. Region 4 Stars Showing High Velocity Low Ionization Components

Star	Fe II 1608	Fe II 2382	Fe II 2585	Fe II 2599	Mg II 2795	Mg II 2802	Mn II 2576	Mn II 2593	Mn II 2605
HD 76534			-72		-64	-64			

Table 3. Region 5 Stars Showing High Velocity Low Ionization Components

Star	Si II 1260	Si II 1304	Si II 1526	Si II 1808	C II 1334	C II 1335	Al II
HD 69882		(-81)			-124,-77	-132,-91	+66
HD 69648					-77	+46	
HD 70309			+104		+84	+84	

Table 3. Region 5 Stars Showing High Velocity Low Ionization Components

Star	Fe II 1608	Fe II 2382	Fe II 2585	Fe II 2599	Mg II 2795	Mg II 2802	Mn II 2576	Mn II 2593	Mn II 2605
HD 69648					-61	-54			

Table 2. Middle Stars Showing High Velocity Low Ionization Components

Star	Si II 1260	Si II 1304	Si II 1526	Si II 1808	C II 1334	C II 1335	Al II
HD 72537	+10,+47		+157			+162	-45,+81
HD 72798	+108	+150		-193,+126	(-459),(+414)		
HD 74319				-40			(-36)
HD 74194	-42				-150,-17	-50	

Table 3. Middle Stars Showing High Velocity Low Ionization Components

Star	Fe II 1608	Fe II 2382	Fe II 2585	Fe II 2599	Mg II 2795	Mg II 2802	Mn II 2576	Mn II 2593	Mn II 2605
HD 72798		+123	-153					+85	
HD 74319	(-50)	(-68)	(-104)	-65,+68	b	b			
HD 74195	-126			-93					

Table 3. Outside Stars Showing High Velocity Low Ionization Components

Star	Si II 1260	Si II 1304	Si II 1526	Si II 1808	C II 1334	C II 1335	Al II
HD 68273		-125					

Table 3. Outside Stars Showing High Velocity Low Ionization Components

Star	Fe II 1608	Fe II 2382	Fe II 2585	Fe II 2599	Mg II 2795	Mg II 2802	Mn II 2576	Mn II 2593	Mn II 2605
HD 68243					-37				

Table 4. Stars Showing High-Velocity High Ionization Species in their IUE Spectra

Star	Region	Si III	Si IV	C IV	N V
HD 72014	1	+153		-37 +53, +143	(+177) (+37)
HD 72127	1				-76, (+120)
HD 71459	1				(+122)
HD 71336	1		-780	+37, +117, +437	+112
HD 72179	1			-99	
HD 72067	1		(+101)	-87, (+256)	-92
HD 72648	1		-420, -225	(-118),(-233)	(-80)
HD 72350	1			-100, +112, +112, +160	(+650)
HD 72088	1	-96	-87, +104	+123, +58	-96
HD 72089	1		-128, +157	+92	
HD 72555	1		-332	-350, -73, +137, (+402)	
HD 72997	1			-45	
HD 74620	2			-301, -101, +399	
HD 74530	2	-130	-107	-107, -332	-117
HD 74234	2	(+158), (+72)	+155	-325, +106, +155	(-63)
HD 74436	2			-104	
HD 74580	2			+334, -66	
HD 74273	2			+164, -111	
HD 74662	2	-148			

Table 6. Stars Showing High-Velocity High Ionization Species in their IUE Spectra

Star	Region	Si III	Si IV	C IV	N V
HD 74711	3		-240, -97, +103	-1127, -93, +113	-73
HD 75309	3			-66	-78
HD 74773	3			-60, +110, +355	
HD 75821	3	-65, +35, +136	+160, +110, -140	+112	
HD 75149	3	-40, -127, +48			+128
HD 76566	3	-138, -80, +29			-104
HD 72798	M		-794, -97	+111, +404	
HD 73010	M			-103	
HD 74319	M			-35	
HD 72798	M				105
HD 70084	5			(-210), -120, -84	
HD 70309	5	+57	+111, +141		
HD 70930	5			-100, -40	
HD 70084	5				-66
HD 69648	5	-64			
HD 74753	O		+887, -333		-184
HD 67621	O		-80		
HD 67536	O		-550	-550	

The Nature of the Vela Supernova Remnant as Revealed by O VI and C IV Absorption

Highly ionized gas, in particular C IV and O VI, is produced in the interstellar medium in regions with hot (T$\sim 10^6$K) X-ray emitting gas and at the boundaries where hot gas and cooler (T$\sim 10^4$K) gas interact. Supernova remnant shocks produce most of the hot gas in the ISM and, if they are in the correct range of speeds, should produce observable quantities of C IV and O VI absorption. In turn, the column densities of these ions are potentially powerful diagnostics of the shock speed and interstellar environment in which the SNR is evolving. With the advent of FUSE, the power of this diagnostic technique is now available.

Data Analysis

We have FUSE data toward 8 stars behind the Vela SNR, and have developed a data reduction and analysis method that produces reasonably reliable O VI column densities, in spite of the complexities of the FUSE spectra in this region.

Models

In order to gain insight into the observational results, the Vela SNR evolution was modelled using Piecewise Parabolic Method numerical hydrodynamics code. The code is 1-D and incorporates non-equilibrium ionization, radiative cooling, thermal conduction and magnetic pressure.

The initial runs were made using the O VI and C IV data for 3 stars in the western region of the Vela SNR, assuming a uniform ambient medium. The result, after constraining the size and shock speed to known values, was unusually low explosion energy. This inconsisency can be overcome by assuming the supernova goes off in a cavity created by the progenitor.

Figures 2-4 present the temperature, velocity, and density profiles from the model runs. Some of the complexity of the hydrodynamics of the transition from adiabatic to radiative can be readily seen. As the shock slows enough that radiative cooling causes the post-shock

gas to cool to T$\sim 10^4$K, the shock loses pressure support and slows. The hot gas behind the shock then catches up with the shock, giving the shock renewed acceleration and resulting in extra compression and cooling in the cool shell. A reverse shock is initiated and propagates back into the hot gas then setting up the reverse shock/contact-discontinuity/forward shock structure familiar from situations in which a shock encounters a higher density medium such as a cloud. In this case it results simply from the dynamics of the transition to a radiative remnant. Note especially that after cooling sets in the hot gas in the remnant has a substantially higher velocity than the gas in the radiative forward shock.

Figure 5 shows the predictions of the numerical hydrodynamic models for the ratio O VI/C IV vs. shock speed. Also plotted are the results of steady radiative shock models kindly provided by John Raymond. The differences between the model results are clearly very large and point to the importance of dynamics in our calculations. A large contributor to the differences is the hot gas inside the remnant that constitutes the sole source of the O VI after the shock has slowed below the speed needed to produce O VI. Another factor is the contribution of the reverse shock to the C IV column, which becomes dominant for shock speeds below $\sim$ 120 km s^{-1}.

Further complications for comparison of observational data to models is demonstrated by Figure 6 which shows the C IV 1548 Å and O VI 1032 Å absorption profiles calculated for a 4 x 10^4 yr after the SN explosion. O VI, coming primarily from hot gas in the remnant, has a single component centered at about 120 km s^{-1}. C IV, on the other hand, comes from both the forward shock and a thin layer on both sides of the reverse shock; thus it has two components. The extremely different nature of the absorption components for C IV and O VI cautions us against any simple component matching analysis of the observational data.

Conclusions

1. C IV and O VI absorption line observations can be powerful diagnostics of SNR characteristics: shock speed, ambient density, age - but interpretation of such results requires careful comparison with detailed models.

2. Steady radiative shock and fully time dependent SNR evolutionary calculations differ markedly in their predictions of C IV and O VI column densities vs. shock speed. This is primarily due to the presence of secondary shocks in the cold shell caused by the dynamics of shell formation and the presence of hot gas behind the cold shell in the SNR bubble.

3. Column densities for O VI and C IV compared to both steady shock models and hydrodynamical SNR modeling, require the shock to be relatively slow ($\sim$100-170 km s^{-1}) to match the data.

Fig. 1.–*FUSE* data for the 1032Å line of O VI (red) and *IUE* data for the 1548Å line of C IV (green) for the three rapidly rotating stars in our *FUSE* dataset. Some or all of the absorption at $\sim$ 120 km s^{-1} and $\sim$ 200 km s^{-1} in the *FUSE* spectra is due to H_2. The *FUSE* data have been binned by a factor of three to increase signal-to-noise.

Fig. 2.–Evolution of the velocity profile in a supernova remnant in our calculation in which we attempt to simulate the Vela SNR. The legend indicates the time after the SN explosion for which each profile corresponds. Note how after 4.0×10^4yr when the cold shell has formed, the fastest moving gas is interior to the shock at the location of the reverse shock. At these times this hot gas interior to the shell, which contains O VI, may have a velocity larger than the outer shock speed.

Fig. 3.–Same as Fig. 2. but the temperature. Note the formation of the cool shell, the thin radiative outer shock and the reverse shock that forms between $t = 3.5 \times 10^4$yr and 4.0×10^4yr after the explosion.

Fig. 4.–Same as Fig. 2. but the density. After formation the cool shell expands over time. The dense cold part of the shell is just behind the forward shock. The contact disconuity can be seen best in the last profile where the density begins to drop behind the outer shock, flattens somewhat then drops again sharply at the inner (reverse) shock.

Fig. 5.–Ion column density ratio vs. shock speed. Here the large differences between the steady shock and hydrodynamical results are demonstrated. The colored dots correspond to the times on Figs. 2–4. The loop in the curve is due to the slowing of the shock after going radiative and subsequent re-acceleration after the hot gas in the expanding bubble catches up with the shock.

Fig. 6.–Absorption profiles for O VI 1032Å (red) and C IV 1548Å (green) calculated from the ionization, density, temperature and velocity profiles from the hydrodynamical simulation at $t = 4.0 \times 10^4$yr. The C IV is concentrated in the forward shock and the reverse shock whereas the O VI comes mostly from the hot gas in the bubble. As a result the absorption profiles are markedly different and peak at different velocities.

Figure 1

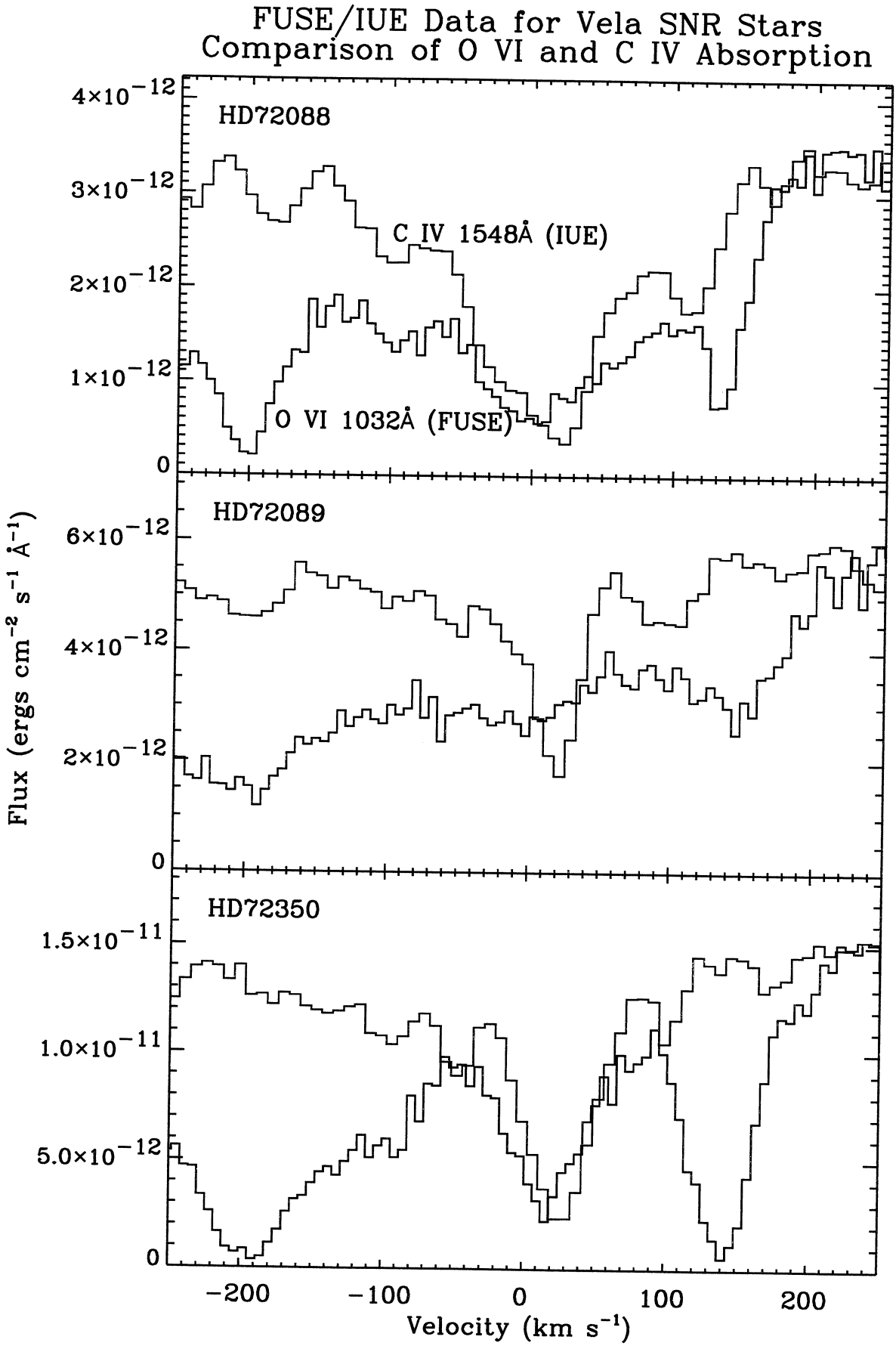
FUSE/IUE Data for Vela SNR Stars
Comparison of O VI and C IV Absorption
HD72088
C IV 1548Å (IUE)
O VI 1032Å (FUSE)
HD72089
HD72350
Flux (ergs cm^{-2} s^{-1} Å^{-1})
Velocity (km s^{-1})
4×10^{-12}
3×10^{-12}
2×10^{-12}
1×10^{-12}
0
6×10^{-12}
4×10^{-12}
2×10^{-12}
0
1.5×10^{-11}
1.0×10^{-11}
5.0×10^{-12}
0
−200
−100
0
100
200

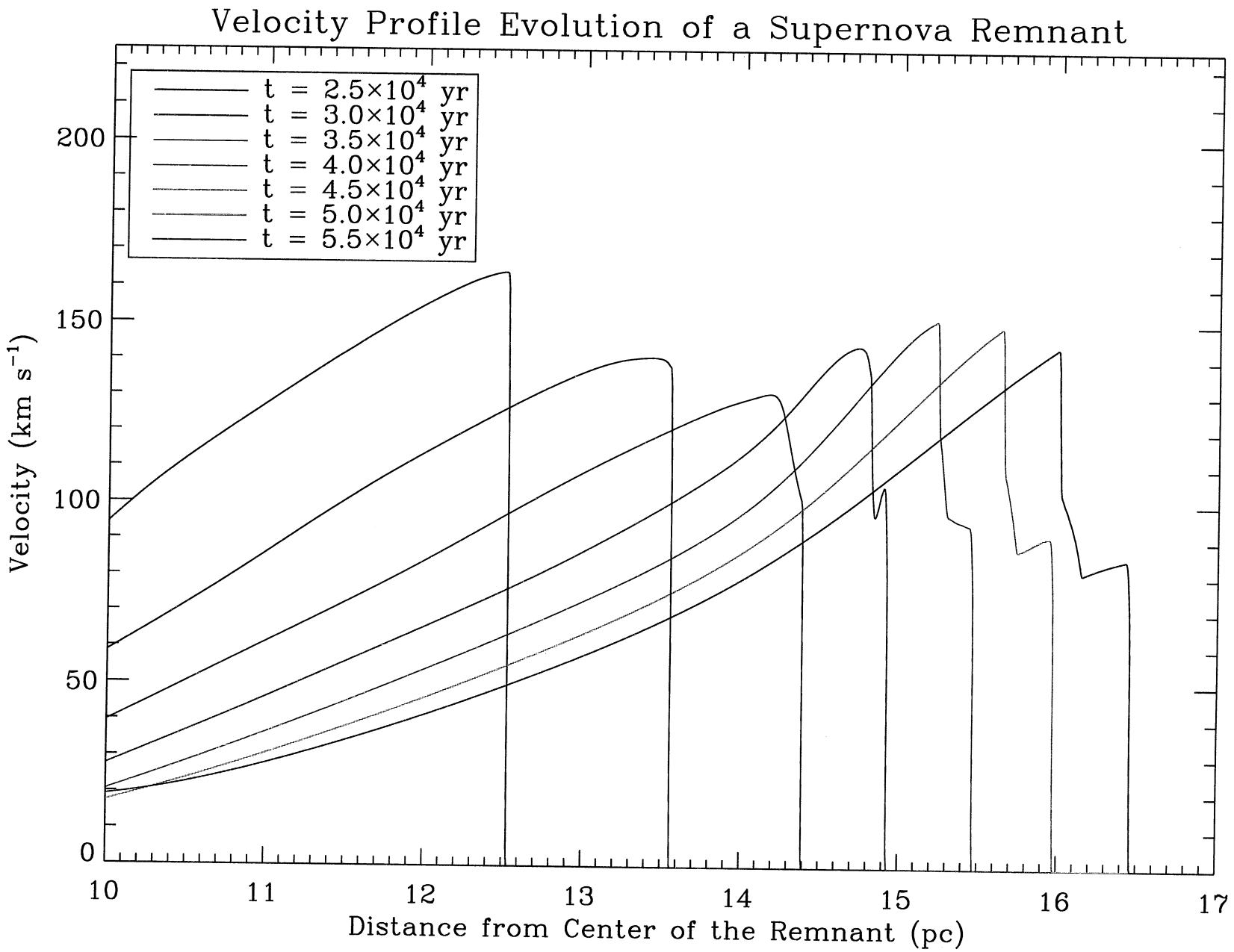
Velocity Profile Evolution of a Supernova Remnant
t = 2.5×10^4 yr
t = 3.0×10^4 yr
t = 3.5×10^4 yr
t = 4.0×10^4 yr
t = 4.5×10^4 yr
t = 5.0×10^4 yr
t = 5.5×10^4 yr
Velocity (km s^-1)
0
50
100
150
200
10
11
12
13
14
15
16
17
Distance from Center of the Remnant (pc)

FIGURE 2

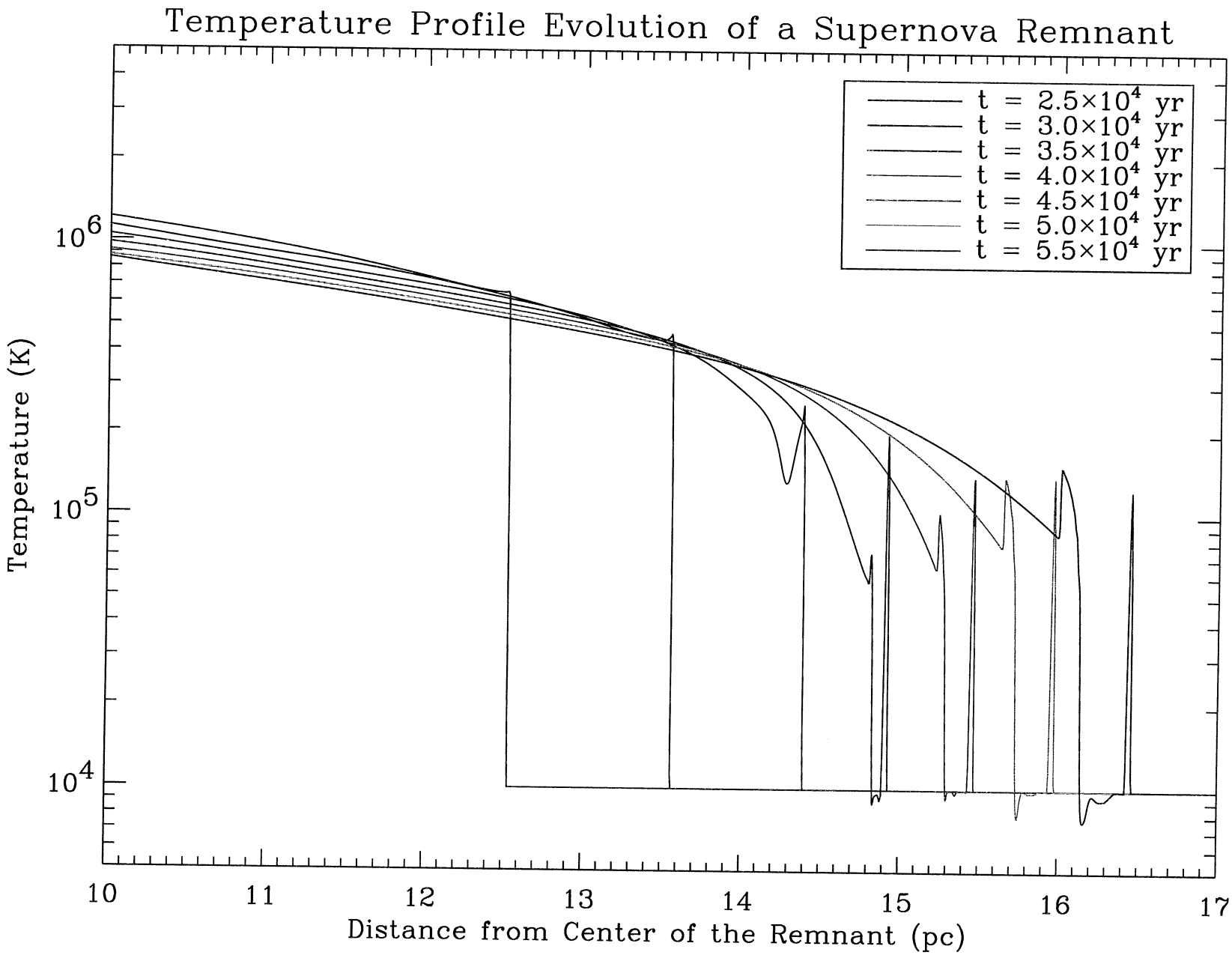
Temperature Profile Evolution of a Supernova Remnant
t = 2.5×10^4 yr
t = 3.0×10^4 yr
t = 3.5×10^4 yr
t = 4.0×10^4 yr
t = 4.5×10^4 yr
t = 5.0×10^4 yr
t = 5.5×10^4 yr
Temperature (K)
10^6
10^5
10^4
10
11
12
13
14
15
16
17
Distance from Center of the Remnant (pc)

Figure 3

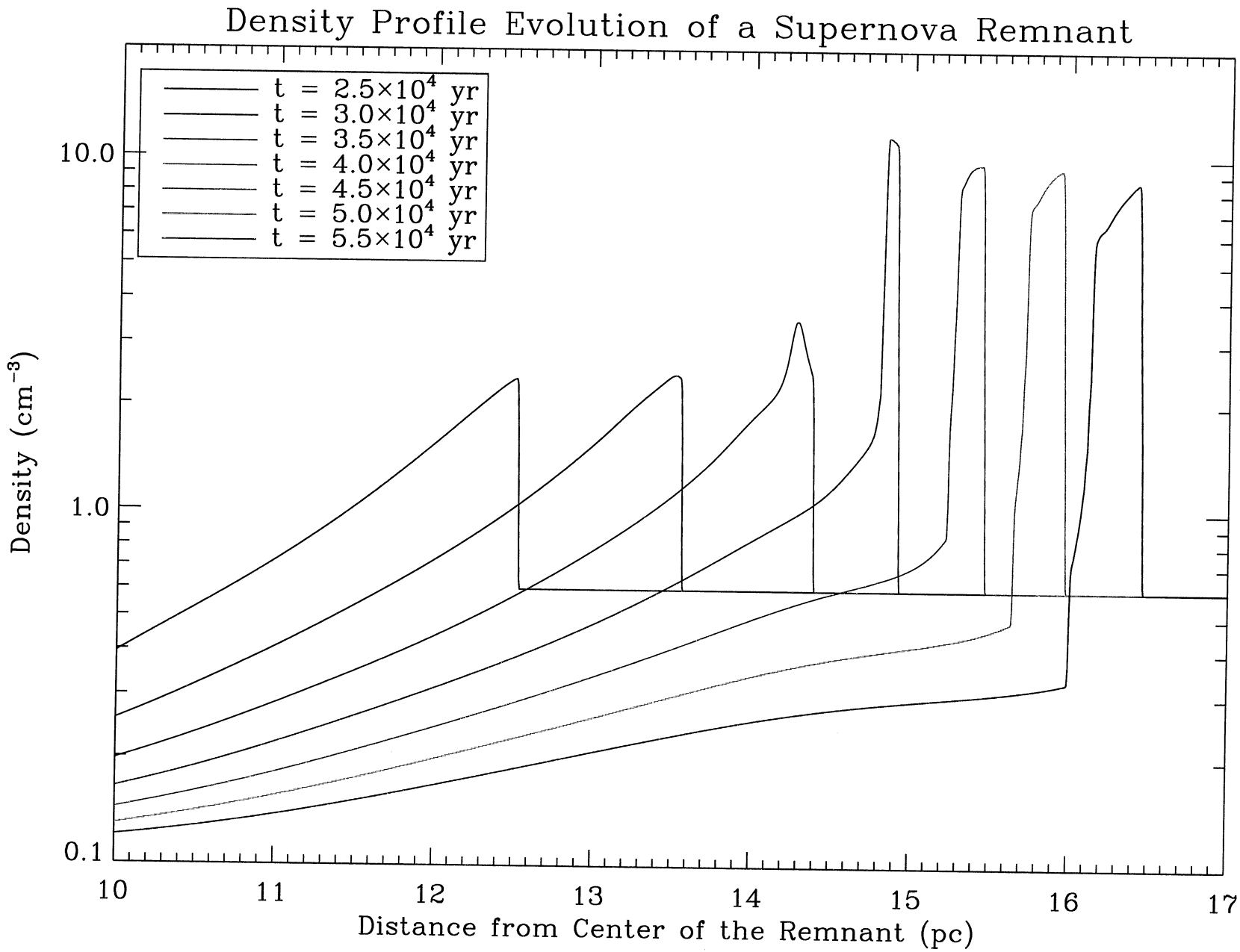
Density Profile Evolution of a Supernova Remnant
t = 2.5×10^4 yr
t = 3.0×10^4 yr
t = 3.5×10^4 yr
t = 4.0×10^4 yr
t = 4.5×10^4 yr
t = 5.0×10^4 yr
t = 5.5×10^4 yr
10.0
1.0
0.1
Density (cm^-3)
10
11
12
13
14
15
16
17
Distance from Center of the Remnant (pc)

Figure 4

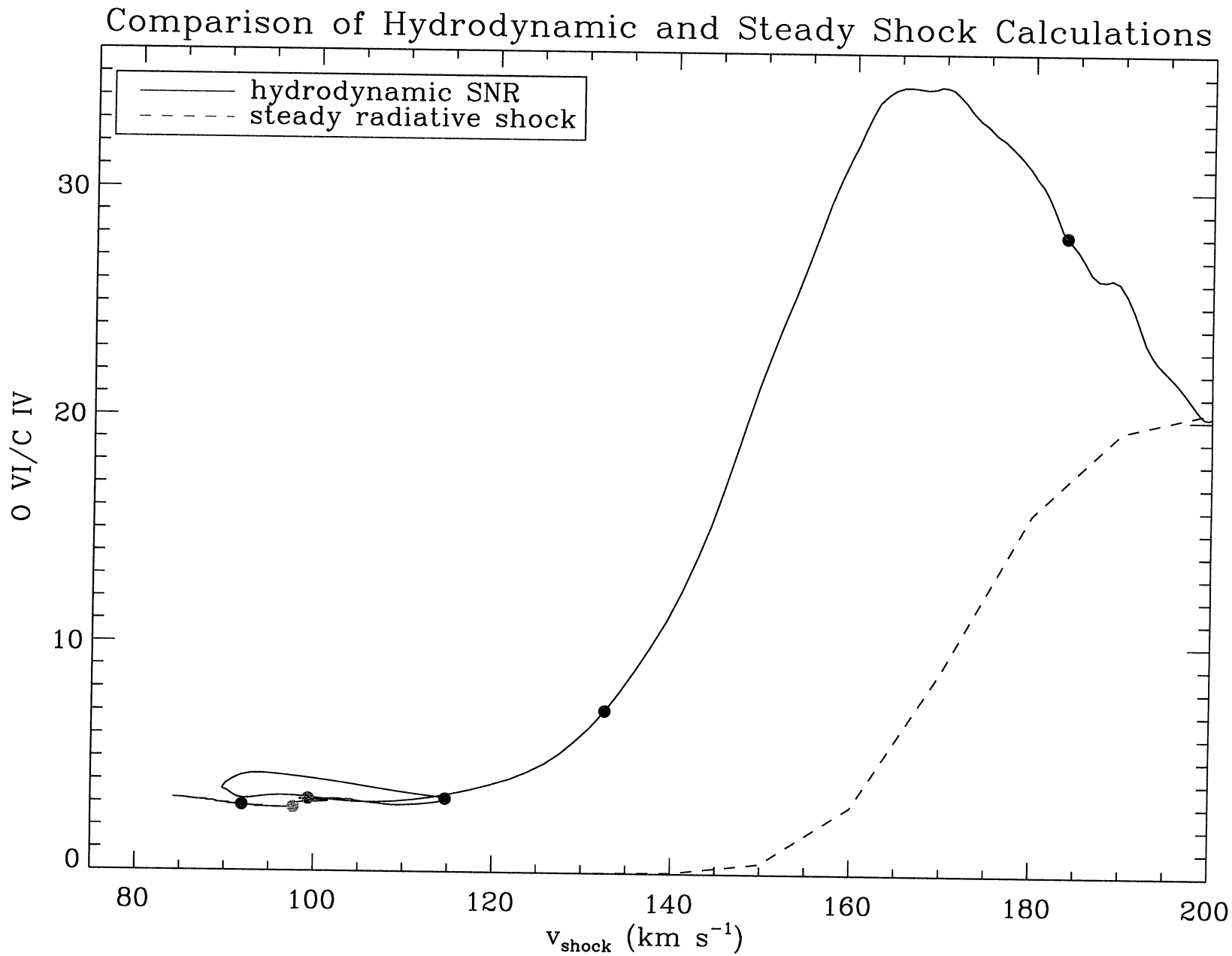
Comparison of Hydrodynamic and Steady Shock Calculations
hydrodynamic SNR
steady radiative shock
O VI/C IV
0
10
20
30
80
100
120
140
160
180
200
v_{shock} (km s^{-1})

Figure 5

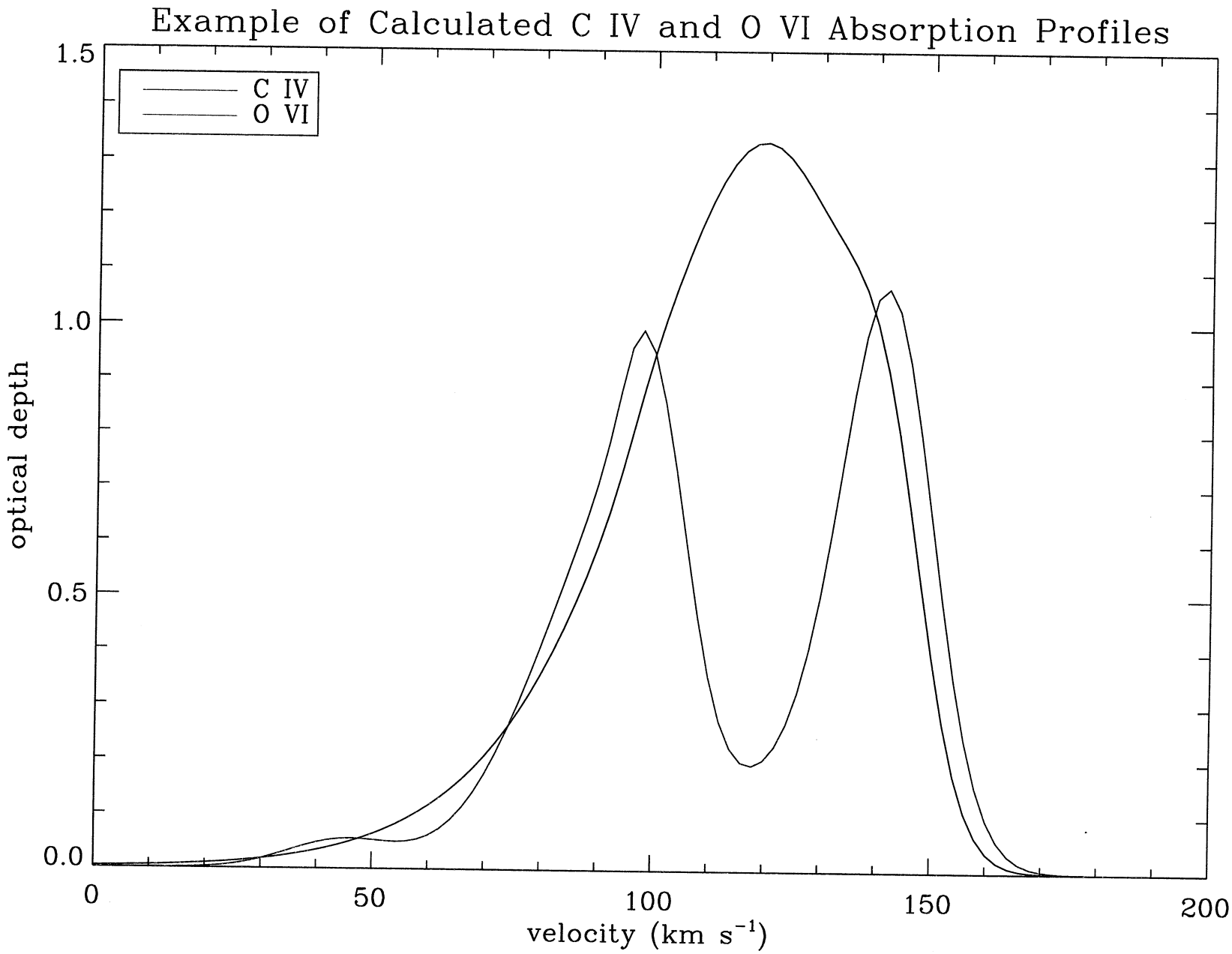
Example of Calculated C IV and O VI Absorption Profiles
C IV
O VI
optical depth
velocity (km s^{-1})
0.0
0.5
1.0
1.5
0
50
100
150
200

Figure 6

Publications

"Survey of UV Absorption Line Data of the Galactic Plane", Nichols, J., Slavin, J., & Anderson, C. 2001, AAS Meeting 198, 59.09.

"Absorption Line Studies of the Elongated Cyg OB1 Superbubble", Lauer, J., Nichols, J., & Slavin, J. 2001, AAS Meeting 199, 65.03.

"The Nature of the Vela Supernova Remnant as Revealed by O VI and C IV Absorption Lines", Nichols, J., Slavin, J., & Anderson, C. 2001, AAS Meeting 1999, 126.12.

"Ultraviolet Absorption Line Study of the Vela Supernova Remnant", Nichols, J. & Slavin, J. 2002, in preparation.

"FUSE Observations of Highly Ionized Gas in the Vela Supernova Remnant", Slavin, J. & Nichols, J. 2002, in preparation.

"The Frequency and Distribution of High Velocity Gas in the Galactic Plane", Nichols, J., Slavin, J., & Anderson, C. 2002, in preparation.